M R S Internet Journal of Nitride Semiconductor Research

Volume 2, Article 22

AlGaN-Based Bragg Reflectors

O. Ambacher, M. Arzberger, D. Brunner, H. Angerer, F. Freudenberg
Walter Schottky Institut, Technische Universität München

N. Esser, T. Wethkamp, K. Wilmers, W. Richter
Institut fuer Festkoeperphysik, Technische Universitaet Berlin

M. Stutzmann
Walter Schottky Institut, Technische Universität München

This article was received on June 11, 1997 and accepted on August 28, 1997.

Abstract

We have studied the dependence of the absorption edge and the refractive index of wurtzite $Al_xGa_{1-x}N$ films on composition using transmission, ellipsometry and photothermal deflection spectroscopy. The Al molar fraction of the $Al_xGa_{1-x}N$ films grown by plasma-induced molecular beam epitaxy was varied through the entire range of composition ($0 \le x \le 1$). We determined the absorption edges of $Al_xGa_{1-x}N$ films and a bowing parameter of 1.3 ± 0.2 eV. The refractive index below the bandgap was deduced from the interference fringes, the dielectric function between 2.5 and 25 eV from ellipsometry measurements. The measured absorption coefficients and refractive indices were used to calculate the design and reflectivity of AlGaN-based Bragg reflectors working in the blue and near-ultraviolet spectral region.

1. Introduction

In spite of recent successes in device development, [1], [2], [3], very little is known about the optical constants of the $Al_xGa_{1-x}N$ system, especially for Al contents larger than 50 %. Following a quite extensive analysis of $Al_xGa_{1-x}N$ grown by molecular beam epitaxy by Yoshida et al. [4] more than a decade ago, significant improvements concerning deposition techniques and the structural quality of epitaxial films have been made, so that a critical revision of the optical constants in the AlGaN alloy system is certainly justified. A precise knowledge of optical constants is particulary important in view of the use of AlGaN films in optical filters, light-emitting and laser diodes.

The fabrication of highly reflective and smooth mirrors for a horizontal cavity laser based on hexagonal Group-III nitrides on sapphire substrate is complicated because of the difficulty of cleaving for parallel mirrors. Therefore a vertical cavity surface emitting laser (VCSEL) operating from the UV to the blue spectral region could be recognized as a useful device for optical imaging systems such as full-color display panels, high density optical recording and photolithography [5].

Highly reflective mirrors are required for blue-emitting low-threshold laser operation and can be realized by dielectric multilayer mirrors or AlGaN-based Bragg reflectors. Nakamura et al. realized stripe- and ridge-geometry InGaN multi-quantum well laser diodes, which showed stimulated emission at a wavelength of 411 nm under pulsed current injection at room temperature [6]. High-reflection facet coatings (reflectivity 70%) composed of 4 pairs of quarter-wave TiO_2/SiO_2 dielectric multilayers were used to reduce the threshold current. The absorption edge of TiO_2 is about 3.1 eV (400 nm) and therefore can not be used for the fabrication of mirrors or filters working in the near UV. AlGaN Bragg reflectors for GaN-based VCSELs can be fabricated using $Al_{x1}Ga_{1-x1}N/Al_{x2}Ga_{1-x2}N$ alternating layers, which can be deposited monolithically during the epitaxial growth of the laser diode.

https://doi.org/10.1557/S1092578300001484 Published online by Cambridge University Press

To calculate the design and the reflectivity of Bragg reflectors for different emission wavelengths of the laser diodes, the refractive index for $Al_xGa_{1-x}N$ is needed. Therefore we have determined the refractive index from transmission and ellipsometry measurements. To evaluate the bandgap and to take the self-absorption of the Bragg reflectors into account, the absorption coefficients of epitaxial AlGaN films covering the whole range of composition were also determined.

2. Experiments

Epitaxial films of $Al_xGa_{1-x}N$ were grown on c-plane sapphire by plasma-induced molecular beam epitaxy (PIMBE). The Al molar fraction x was varied in approximately equidistant steps between $0 \leq x \leq 1$. Conventional Al and Ga effusion cells and a r.f.-plasma source (Oxford Applied Research CARS) for nitrogen radicals were used in the deposition process. The nominally undoped epitaxial films were grown without a buffer layer at temperatures between 810 °C and 1000 °C. The FWHM of the (002) rocking curve observed by X-ray diffraction increased from 0.18° to 0.43° by increasing the Al content from x = 0 to x = 0.8. For alloys with x > 0.8, the substrate temperature was changed from 810 to 1000 °C, which resulted in improved structural properties of the films and a FWHM rocking curve of 0.2° [7]. The thickness (≈1 μm) and the growth rate (between 0.5 and 0.6 μm/h) of the films were determined by scanning electron microscopy with an accuracy of ±10 nm [8]. The $Al_xGa_{1-x}N$ films had rms surface roughnesses between 5 and 15 nm, as obtained by atomic force microscopy. The Al molar fraction was examined by elastic recoil detection analysis (ERDA) [9]. The ERDA measurements were generaly in good agreement with estimates based on the lattice constants a_0 and c_0 (taking into account a biaxial stress, $\sigma \leq$ 0.4 GPa), obtained by high resolution X-ray diffraction (HRXRD) using Vegard's law [7], [10].

In order to determine the absorption coefficient versus photon energy at room temperature, photothermal deflection spectroscopy (PDS) [11], [12] and transmission measurements, using a Perkin Elmer Lambda 900 double beam spectrometer with a resolution of 1 nm, have been carried out in the spectral range from 195 nm to 2000 nm. For the calculation of the absorption coefficient α from the transmission data, we used the procedure described by Freeman and Paul [13]. The reflectivity between the epitaxial AlGaN film and the sapphire substrate was determined using the results of Malitson, who developed a Sellmeir equation to permit calculation of the index of refraction of sapphire between 200 and 6000 nm. The index of refraction, n, of the Group-III nitrides was obtained from examination of interference fringe minima and maxima in the transmission spectrum [8].

The dielectric function of the epitaxial AlGaN films were measured in the spectral range 3-25 eV using an ellipsometer operating with synchrotron radiation at the Berlin electron storage ring BESSY I [14]. A more detailed description of the general experimental design, the beamline polarization and the polarization properties of the triple-reflection-analyser is given in Ref. [15].

3. Results and Discussion

3.1. Dependence of the Absorption Edge on the Al molar Fraction

Figure 1 shows the transmission measurements of different epitaxial $Al_xGa_{1-x}N$ films versus photon energy at room temperature. To determine the bandgap of the samples, the absorption coefficients α of the AlGaN films were calculated from the transmission and PDS measurements, Figure 2. The effective bandgap of the $Al_xGa_{1-x}N$ films was defined as the photon energy $E_{4.8}$ at which the absorption coefficient equals a value of $10^{4.8}$ cm^{-1}. The physical justification for this definition is given by photoluminescence and reflection measurements of GaN, showing that $E_{4.8}$ lies between the photon energy of the free excitons FX_A and FX_B in the temperature range between 5 K and 300 K [8]. Moreover, the effective bandgap $E_{4.8}$(GaN) follows the temperature dependence of the free excitons and increases from 3.420 eV to 3.480 eV with decreasing temperature from 300 K to 5 K. The energy offset $E_{4.8}$(GaN)-FX_A and $E_{4.8}$(GaN)-FX_B is approximately 2 and -5 meV. With increasing Al content x, the effective bandgap $E_{4.8}$ shifts toward higher energies, following the phenomenological quadratic dependence on the Al molar fraction [16]:

$$E_{4.8}(Al_xGa_{1-x}N) = x\,E_{4.8}(AlN) + (1-x)\,E_{4.8}(GaN) - bx\,(1-x),\ T = 300\ K. \quad (1)$$

For $E_{4.8}$(GaN) and $E_{4.8}$(AlN) we observed 3.42 and 6.13 eV at room temperature. From the energy position of the absorption edge versus Al concentration a bowing parameter $b = 1.3 \pm 0.2$ eV can be determined (see insert in Figure 2). This value agrees within the experimental error with the bowing parameter of 1.0 ± 0.3 eV obtained by Koide [17]. The biaxial stress σ in the samples, due to mismatch of the lattice constants and the thermal

https://doi.org/10.1557/S1092578300001484 Published online by Cambridge University Press

expansion coefficients of the substrate and epitaxial films, was calculated from the results of HRXRD-measurements and is estimated to be below 0.4 GPa. Therefore, an upper limit of 10 meV for the stress-induced shift of the bandgap can be calculated using $dE_g/d\sigma \approx 25$ meV/GPa [18]. As a consequence, an upper limit of the bandgap shift towards higher energies caused by biaxial compressive stress should be approximately 10 meV at room temperature.

3.2. Index of refraction

In Figure 3 the index of refraction (calculated from transmission measurements) versus photon energy is shown for different $Al_xGa_{1-x}N$ films (T = 300 K) in the range between 1.5 and 5.5 eV. The expected increase of the index of refraction with increasing photon energy towards the bandgap, and the overall decrease with Al content, is observed for the whole series of samples. The dependence of refractive index on energy obtained for the GaN and the $Al_{0.1}Ga_{0.9}N$ samples is in excellent agreement with the results of Amano et al. [19], [20] and Vidal et al. [21]. For $0.7 < x < 1$ there is a tendency for the experimentally determined refractive indexes to be too low, most probably due to a decrease of the effective film density compared to an ideal crystal. Thus, a decrease of the index of refraction for example from 2.05 to 2.00 would require a density deficit of approximately 2 %.

For the case of the direct absorption edge of $Al_xGa_{1-x}N$ films the index of refraction can be calculated for energies lower than the bandgap by [22]:

$$n^2(h\nu,x) = \varepsilon_r(h\nu,x) = C(x) + A(x)y^{-2}(2 - (1+y)^{1/2} - (1-y)^{1/2}), \quad (2a)$$

where:

$$A(x) = 4\pi\, m_e^{-2}\nu^{-2}h^{-3}e^2\,(2\mu(x))^{3/2}\,|P_{CV}(x)|^2\,E_g(x)^{1/2},\ C(x) \text{ is a const.}(x),\ \mu = m_V m_C/m_V+m_C,\ y = h\nu/E_g(x), \quad (2b)$$

ε_r is the dielectric function, m_C and m_V are the effective masses of the conduction and valence band, m_e and e are the electron mass and charge, C is photon energy independent for a fixed Al-content, hν is the photon energy, $8\pi^2|P_{CV}(x)|^2/m_e h\nu$ is the oscillator strength of the optical transition and $E_g(x)$ is the direct bandgap of $Al_xGa_{1-x}N$. We used equation (2.a) to fit the measured index of refraction $n(h\nu,x)$ for different $Al_xGa_{1-x}N$ films, by using the measured effective bandgap $E_{4.8}(x) = E_g(x)$ and A(x) and C(x) as fitting parameters. We found a linear increase of C(x) with increasing Al-content of the films and a square root dependence of A(x) (motivated by (2a): $A(x) \propto E_g(x)^{1/2} \propto x^{1/2}$) which can be described by the following equations:

$$C(x) = -(2.2\pm0.2)\,x + (2.66\pm0.12), \text{ and (3a) } A(x) = (3.17\pm0.39)\,x^{1/2} + (9.98\pm0.27). \quad (3b)$$

The combination of the equations (2a), (3a) and (3b) provides an analytical relation for the index of refraction as a function of photon energy ($h\nu < E_g$) and Al content ($0 \le x \le 1$).

The reflectivity of the AlGaN films above the bandgap ($h\nu \ge E_g$) can be calculated from ellipsometry mesurements, which allow the determination of the effective dielectric function $\langle\varepsilon(h\nu)\rangle = \langle\varepsilon_1(h\nu)\rangle + i\langle\varepsilon_2(h\nu)\rangle$. The quantity $\langle\varepsilon_2(h\nu)\rangle$ is a measure of the absorption and is related to the joint density of states. It therefore is directly connected with the electronic bandstructure of the material [14]. The refractive index $n(h\nu) = n(h\nu) + ik(h\nu)$ and the reflectivity were calculated using the equations: $\varepsilon_1 = n^2 - k^2$, $\varepsilon_2 = 2nk$. In Figure 4 and Figure 5, the dielectric functions of GaN and AlGaN are shown in the energy region between 2.5 and 17 or 25 eV.

Below the fundamental gaps, Fabry-Perot interferences were observed and the absorption maxima labeled with E_1, E_2 and E_3 could be associated with interband transitions at specific points or regions of the Brillouin zone (discussed in more detail in Ref. [14], [23] and [24]). The calculated absorption coefficients and reflectivities of the GaN and AlGaN films for photon energies above the bandgap can be applied to determine the influence of thin buffer layers on the optical properties of AlGaN-based Bragg reflectors and filters.

3.3. AlGaN-based Bragg Reflectors

The measured refractive index difference of AlN and GaN is comparable to that of AlAs and GaAs [25]. Therefore,

https://doi.org/10.1557/S1092578300001484 Published online by Cambridge University Press

AlGaN-based Bragg reflectors (DBR) are considered to be suitable for mirrors for the GaN-based VCSEL operating in the UV spectral regions.

When calculating the design of Bragg reflectors for different wavelengths, two limitations for practical $Al_{x1}Ga_{1-x1}N/Al_{x2}Ga_{1-x2}N$ stacked layers have to be taken into account. First the self-absorption of the reflector for a given wavelength $\alpha(x_1)md_{x1}$ ($\alpha(x_1)$: absorption coefficient of $Al_{x1}Ga_{1-x1}N$, m: number of periods of the DBR, d_{x1}: thickness of one $Al_{x1}Ga_{1-x1}N$ layer) has to be below 10^3 to achieve reflectivies above 90%. This limits the minimum Al content of the $Al_{x1}Ga_{1-x1}N$ layers with the lower bandgap. We determined x_1, assuming that the dependence of the absorption coefficient on photon energy for the AlGaN films (determined by PDS and transmission spectroscopy) are also valid for stacked layers with thicknesses between 30 and 60 nm. Stress or quantum confinement effects will cause a shift of the bandgap to higher energies and will require raising the Al content x_1. Stress-induced defects or high defect densities at the interfaces of the DBR will cause an increase of subbandgap absorption and require an increase of x_1, which was not taken into consideration in our calculation. Second, the lattice mismatch $(a_0(x_1)-a_0(x_2))/a_0(x_1)$ between the $Al_{x1}Ga_{1-x1}N$ and $Al_{x2}Ga_{1-x2}N$ layers was chosen to be equal or below 1%, which is a prerequisite for epitaxial growth of heterostructures with 20 or more periods of $Al_{x1}Ga_{1-x1}N/Al_{x2}Ga_{1-x2}N$ layers. This assumption limits the maximum Al content x_2 for a given x_1 or a given wavelength λ at which the reflectivity of the DBR should have a maximum.

The theoretical reflectivity of the DBRs for different wavelength was calculated using Equations 2 and 3 for the wavelength dependence of the refractive index for different AlGaN compositions applying a matrix method for the multilayer system [26]. The structure of the calculated DBRs consisted of periodically repeated $Al_{x1}Ga_{1-x1}N/Al_{x2}Ga_{1-x2}N$ layers grown on a c-plane sapphire substrate, using a 20 nm thick GaN buffer layer. In Figure 6, the Al contents x_1 and x_2 are shown versus wavelength, which were calculated (under consideration of self-absorption and lattice mismatch) to give the highest reflectivity. Below 370 nm, the Al contents x_1 and x_2 increase with decreasing wavelength. At 290 nm, x_2 reaches the value for AlN and a further increases of photon energy causes a decrease in the difference between the refractive indices $n(x_1)$ and $n(x_2)$ and in the reflectivity. Above 390 nm, Bragg reflectors with the highest reflectivity can be fabricated by growing $Al_{0.5}Ga_{0.5}N/Al_{0.91}Ga_{0.09}N$ heterostructures. With increasing wavelength the maximum reflectivity R_{max} can be reached only by increasing the thicknesses of the AlGaN layers.

The Al contents of DBRs already realized by Redwing et al. [27] and Kung et al. [25] are given for comparision. The thicknesses d_1 and d_2 of the corresponding $Al_{x1}Ga_{1-x1}N$ and $Al_{x2}Ga_{1-x2}N$ quarter-wavelength layers are given in Figure 7. Above 390 nm the optimal thicknesses d_1 and d_2 increase linearly with increasing wavelength for fixed Al contents. Kung et al. [25] used 20 periods of Si-doped $Al_{0.2}Ga_{0.8}N/Al_{0.5}Ga_{0.5}N$ multilayers grown on an AlN buffer layer. By changing the thickness of the layers, Bragg reflectors for 456, 409 and 369 nm were realized. We calculated the quarter wavelength thicknesses of the AlGaN layers for this case to be between 36.2 and 47.6 nm for d_1 and between 39.6 and 50.7 nm for d_2, increasing linearly with the wavelength. Peak reflectivities of higher than 60 % were estimated by Kung [25] from dips in transmission measurements at room temperature. By the matrix method, we calculated maximum reflectivities from 45% to 75% for wavelengths from 456 to 369 nm (Figure 8).

By realizing $Al_{0.5}Ga_{0.5}N/Al_{0.91}Ga_{0.09}N$ DBR structures, the reflectivities should be improved to between 83% and 94% for 20 periods and between 97% and 99.6 % for 30 periods in the same range of wavelength. Maximum reflectivities R_{max} above 98% or 99.8% can be realized between 310 and 350 nm with 20 or 30 periods of AlGaN layers. For photon energies above 4.2 eV, the reflectivity of the AlGaN-based Bragg reflectors decreases drastically, indicating an upper photon energy limit for laser operation that can be realized by AlGaN VCSELs.

To test the validity of our model and the measured indices of refraction of the AlGaN layers, the transmission curves of Bragg reflectors measured by Kung et al. [25] were simulated. From the published data of $x_1 = 0.2$ and $x_2 = 0.5$, we calculated the refractive index and the quarter-wave thicknesses of the AlGaN layers for the wavelengths of 456, 409 and 369 nm. The matrix method provides the reflectivity R_{max} in dependence of the photon energy. The measured transmission spectra of the Bragg reflectors and the calculated transmission ($T(h\nu) = 1-R_{max}(h\nu)$) are shown in Figure 9. The measured transmission spectra are in good agreement with the calculated results, indicating the validity of the applied model and the accuracy of the measured refractive indices shown in Figure 3.

https://doi.org/10.1557/S1092578300001484 Published online by Cambridge University Press

4. Conclusion

In summary the influence of the Al content on the optical properties of epitaxial $Al_xGa_{1-x}N$ layers deposited by plasma-induced MBE on sapphire substrates has been studied by combining transmission, ellipsometry and photothermal deflection spectroscopy measurements. The absorption edge was varied between 3.42 and 6.13 eV by changing the Al content of the epitaxial $Al_xGa_{1-x}N$ films. The corresponding bandgap value obeys a quadratic relation with a bowing parameter of 1.3 0.2 eV. From the interference fringes obtained in transmission and from ellipsometry measurements, the index of refraction and the reflectivity was determined in dependence of Al content and photon energy. Using a formalism based on the Kramers-Kronig-dispersion relation, a full set of equations is given to describe the refractive index of AlGaN for photon energies below the bandgap. The determined optical properties provide an experimental basis for the design of optical filters and Bragg reflectors. By applying a matrix method for multilayer systems the design of optimized Bragg reflectors and their reflectivity were calculated, providing for the fabrication of DBRs working in the range of wavelength between 450 and 300 nm.

Acknowledgments

The authors would like to thank M. Kelly for helpful discussions. The work was supported by the Deutsche Forschungsgemeinschaft (Stu 139/3-1) and the Bayerische Forschungsstiftung (FOROPTO II).

References

[1] Barbara Goldenberg, J. David Zook, Robert J. Ulmer , *Appl. Phys. Lett.* ***62***, 381-383 (1993).

[2] Shuji Nakamura, Takashi Mukai, Masayuki Senoh , *Appl. Phys. Lett.* ***64***, 1687-1689 (1994).

[3] S Nakamura, M Senoh, S Nagahama, N Iwasa, T Yamada, T Matsushita, H Kiyoku, Y Sugimoto, *Jpn. J. Appl. Phys.* ***35***, L74-L76 (1996).

[4] S. Yoshida, S. Misawa, S. Gonda, *J. Appl. Phys.* ***53***, 6844 (1982).

[5] T Honda, A Katsube, T Sakaguchi, F Koyama, K Iga, *Jpn. J. Appl. Phys.* ***34***, 3527-3532 (1995).

[6] S. Nakamura, M. Senoh, S. Nagahama, N. Iwasa, T. Yamada, T. Matsushita, Y. Sugimoto, H. Kiyoku, *Appl. Phys. Lett.* ***69***, 1477-1479 (1996).

[7] H. Angerer, O. Ambacher, R. Dimitrov, Th. Metzger, W. Rieger, M. Stutzmann, *MRS Internet J. Nitride Semicond. Res.* ***1***, 15 (1996).

[8] D Brunner, H Angerer, E Bustarret, F Freudenberg, R Hˆpler, R Dimitrov, O Ambacher, M Stutzmann, unpublished (1997).

[9] H Angerer, D Brunner, F Freudenberg, O Ambacher, M Stutzmann, R Hˆpler, T Metzger, E Born, G Dollinger, A Bergmaier, S Karsch, HJ Kˆrner, unpublished (1997).

[10] L Vegard, *Z. Phys.* ***5***, 17 (1921).

[11] O Ambacher, W Rieger, P Ansmann, H Angerer, TD Moustakas, M Stutzmann, *Sol. St. Comm.* ***97***, 365-370 (1996).

[12] O. Ambacher, D. Brunner, R. Dimitrov, M. Stutzmann, F. Scholz, A. Sohmer, unpublished (1997).

[13] E.C. Freeman, W. Paul, *Phys. Rev. B* ***20***, 716-727 (1979).

[14] T. Wethkamp, K. Wilmers, N. Esser, W. Richter, O. Ambacher, H. Angerer, G. Jungk, R.L. Johnson, M. Cardona, unpublished (1997).

[15] J. Barth, R.L. Johnson, M. Cardona, *Handbook of Optical Constants of Solids II* (E. Palik, Academic Press, New York, 1991) .

[16] J.C. Phillips, *Bonds and Bands in Semiconductors* (Academic Press, New York, 1973) .

[17] Y. Koide, H. Itoh, M. R. H. Khan, K. Hiramatu, N. Sawaki, I. Akasaki , *J. Appl. Phys.* ***61***, 4540-4543 (1987).

[18] W Rieger, T Metzger, H Angerer, R Dimitrov, O Ambacher, M Stutzmann, *Appl. Phys. Lett.* ***68***, 970 (1996).

[19] H. Amano, N. Watanabe, N. Koide, I. Akasaki, *Jpn. J. Appl. Phys.* ***32***, L1000-1002 (1993).

[20] I. Akasaki, H. Amano, *Mater. Res. Soc. Symp. Proc.* ***339***, 443-452 (1994).

[21] M. A. Vidal, G. Ramirez-Flores, H. Navarro-Contreras, A. Lastras-Martinez , R. C. Powell, J. E. Greene , *Appl. Phys. Lett.* ***68***, 441-443 (1996).

[22] P.Y. Yu, M. Cardona, *Fundamentals of Semiconductors* (Springer Verlag Berlin, Berlin, 1996) .

[23] S. Logothetidis, J. Petalas , M. Cardona , T. D. Moustakas , *Phys. Rev. B* ***50***, 18017-18029 (1994).

[24] C.G. Olson, D.W. Lynch, A. Zehe, *Phys. Rev. B* ***24***, 4629-4633 (1981).

[25] P. Kung, A. Saxler, D. Walker, X. Zhang, R. Lavado, K.S. Kim, M. Razeghi, *Mater. Res. Soc. Symp. Proc.* ***449***, 79-84 (1997).

[26]S. Rochus, private communication, Dissertation, Technical University Munich, Germany, 1995

[27] Joan M. Redwing , David A. S. Loeber, Neal G. Anderson , Michael A. Tischler, Jeffrey S. Flynn , *Appl. Phys. Lett.* ***69***, 1-3 (1996).

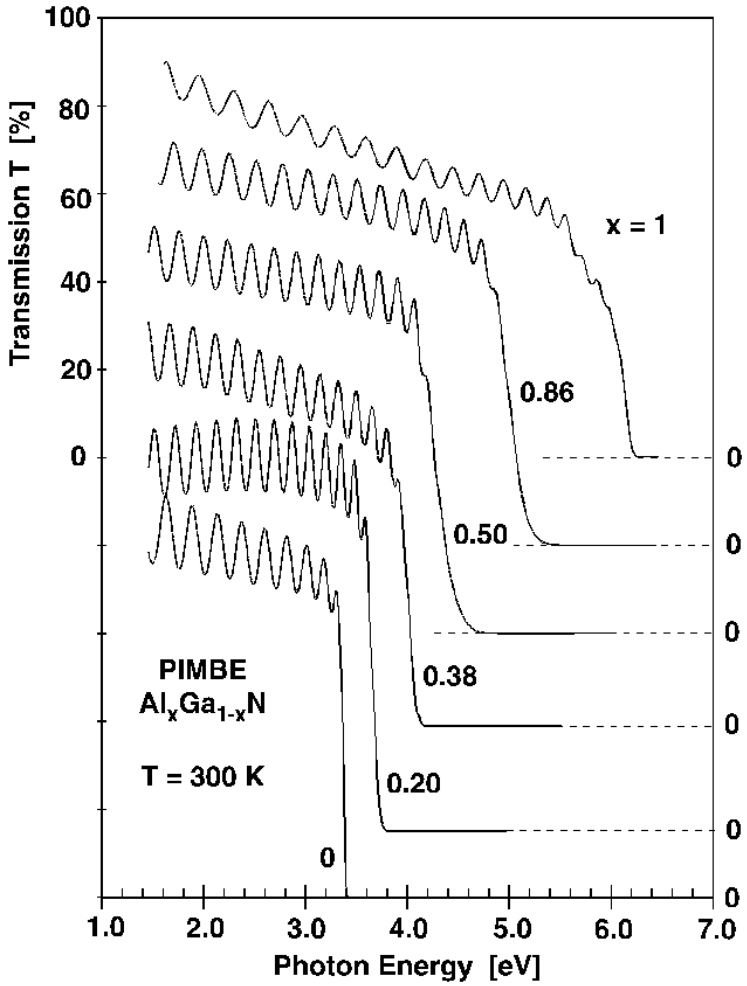

Figure 1. Room temperature transmission measurements of 1 μm thick epitaxial wurtzite AlGaN films grown by plasma-induced molecular beam epitaxy.

https://doi.org/10.1557/S1092578300001484 Published online by Cambridge University Press

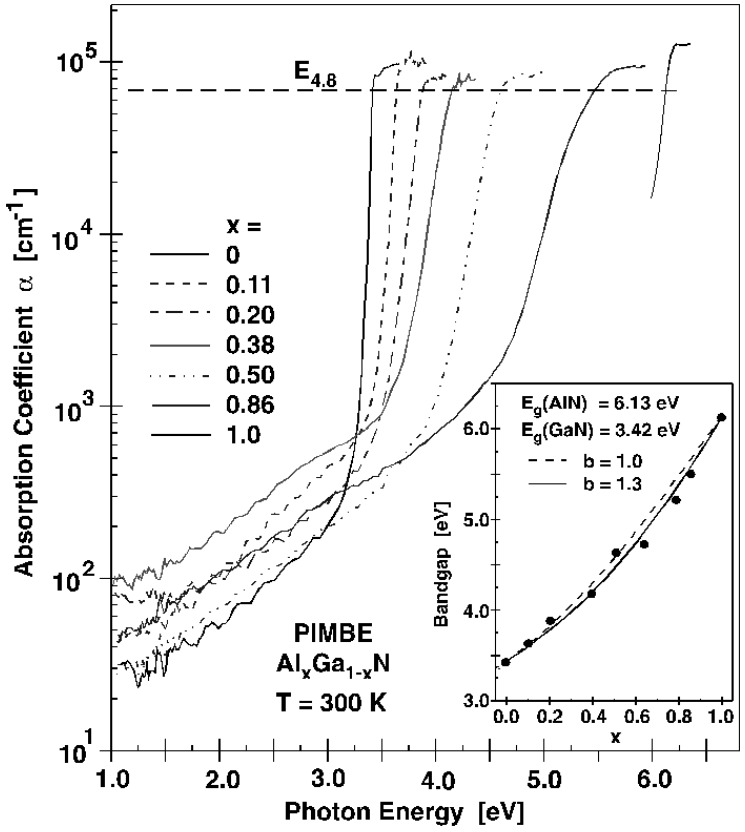

Figure 2. Absorption coefficient α of epitaxial $Al_xGa_{1-x}N$ films versus photon energy measured by transmission and photothermal deflection spectroscopy at room temperature. The insert shows the dependence of the absorption edge determined from $E_{4.8}$ (energy at which the absorption coefficient is equal to $10^{4.8}$ cm^{-1}) versus the Al content of the films.

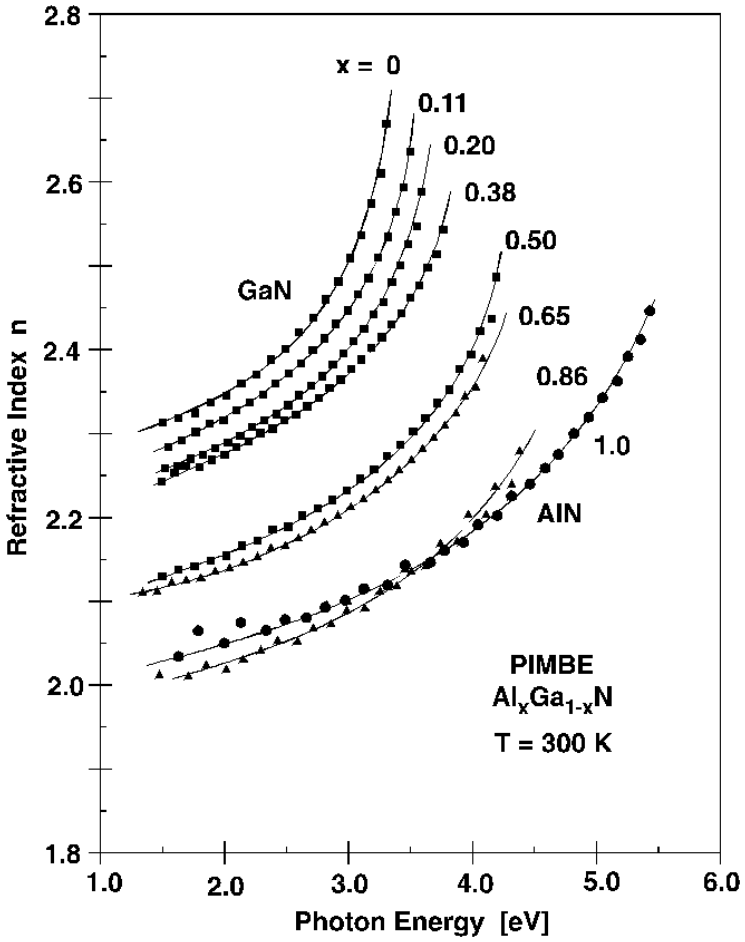

Figure 3. Index of refraction n of different $Al_xGa_{1-x}N$ films versus photon energy at room temperature (solid lines are fits to equation (2a)).

https://doi.org/10.1557/S1092578300001484 Published online by Cambridge University Press

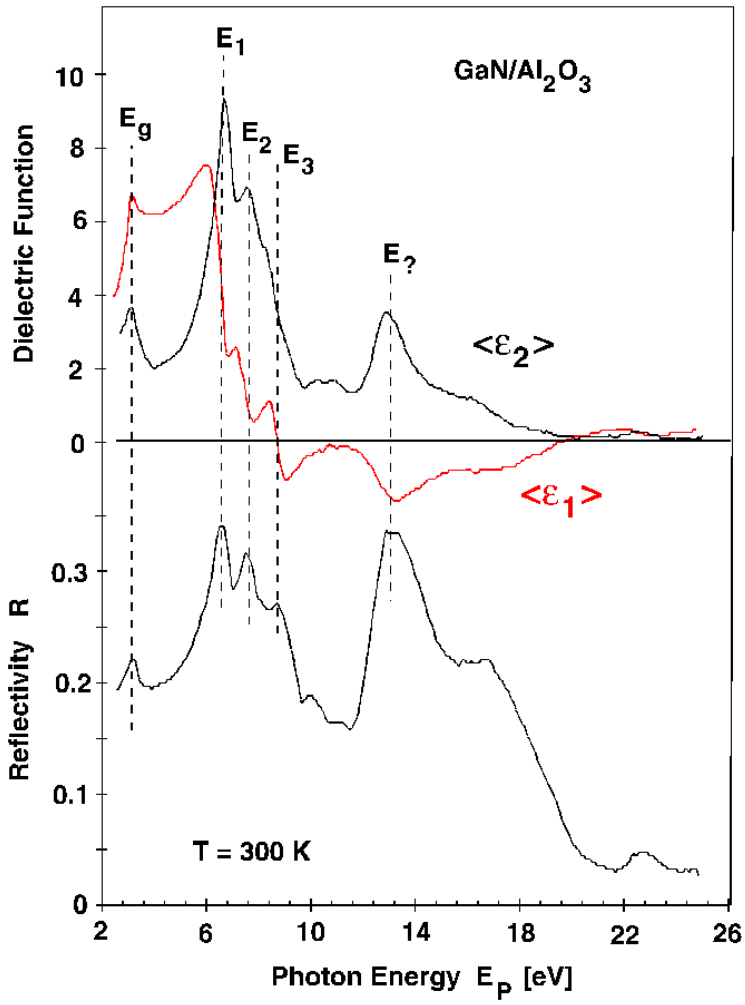

Figure 4. Dielectric functions and reflectivity of GaN. Labeled are the interband transitions E_g, E_1, E_2, and E_3, as well as the broad feature above 13 eV, which is not assigned to one distinct point or region of the Brillouin zone.

https://doi.org/10.1557/S1092578300001484 Published online by Cambridge University Press

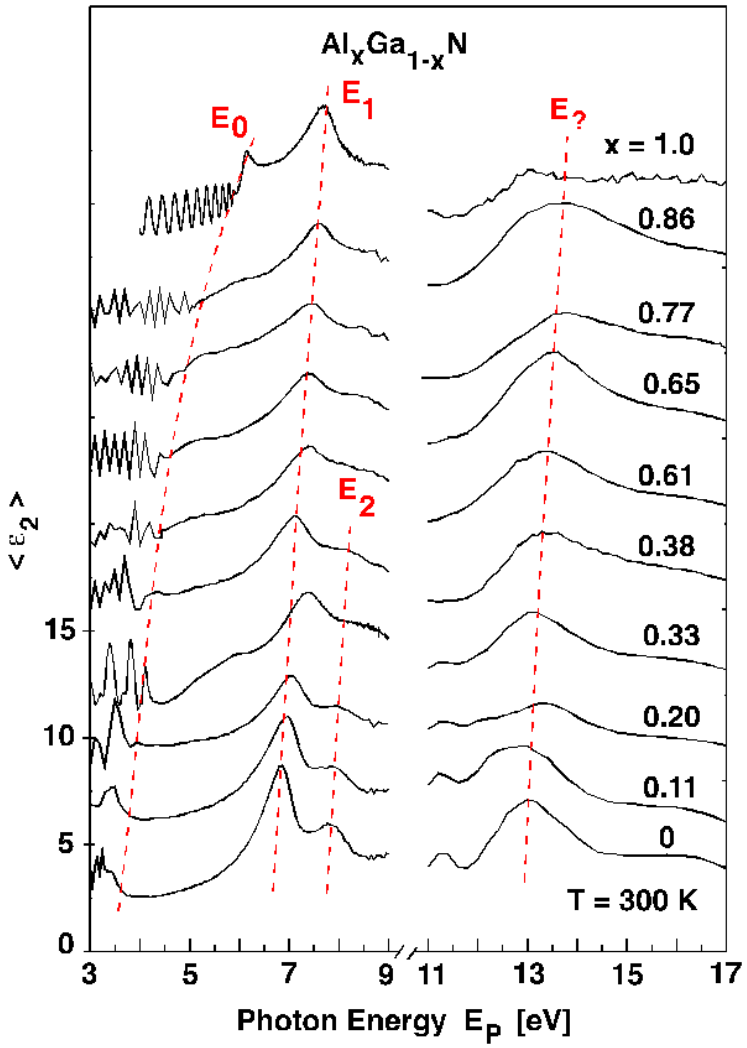

Figure 5. Imaginary parts of dielectric functions of hexagonal AlGaN films. Datasets are shifted for clarity.

https://doi.org/10.1557/S1092578300001484 Published online by Cambridge University Press

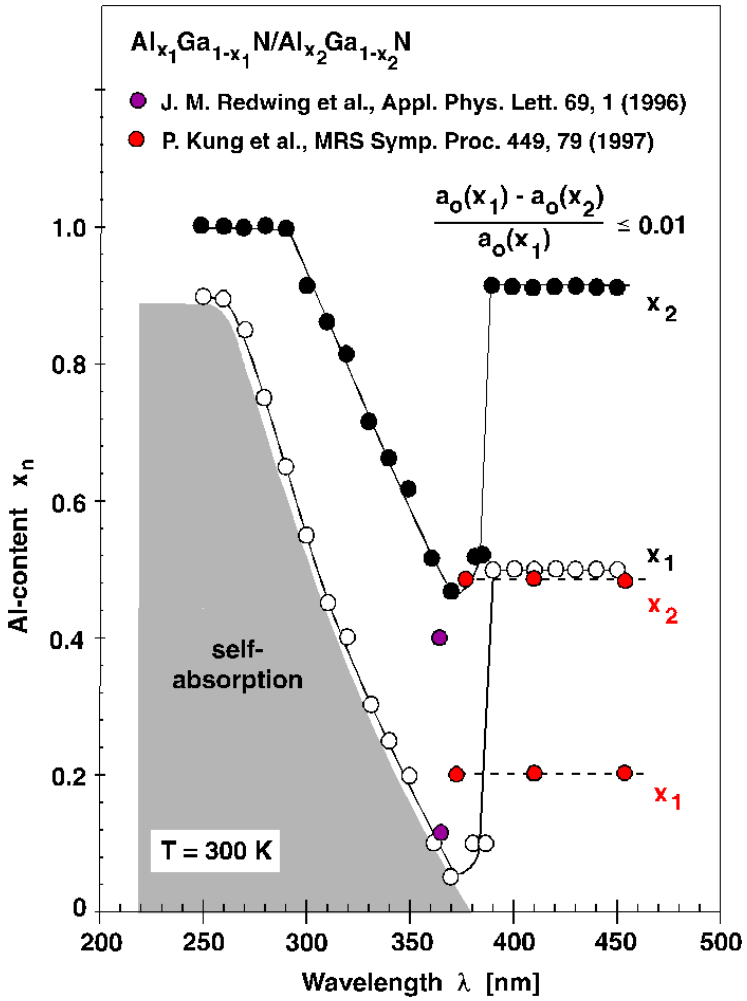

Figure 6. Al content x_1 and x_2 of optimized $Al_{x1}Ga_{1-x1}N/Al_{x2}Ga_{1-x2}N$ Bragg reflectors versus wavelength. The results of Redwing et al. [27] (violet symbols) and Kung et al. [25] (red symbols) are given for comparison.

https://doi.org/10.1557/S1092578300001484 Published online by Cambridge University Press

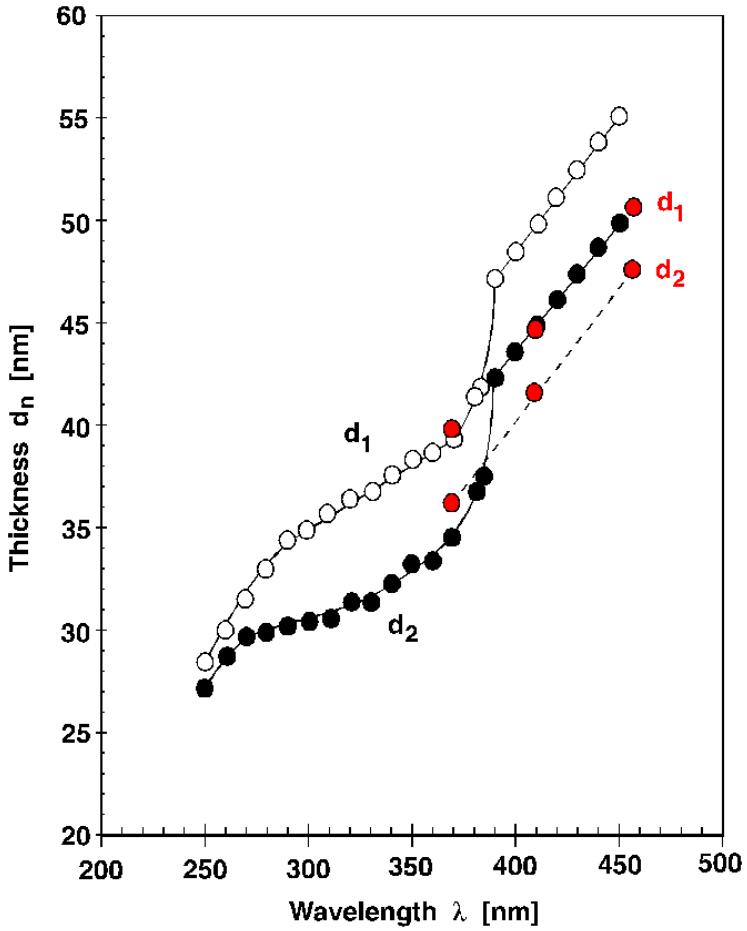

Figure 7. Quarter-wave thicknesses d_1 and d_2 of the optimized $Al_{x1}Ga_{1-x1}N/Al_{x2}Ga_{1-x2}N$ Bragg reflectors versus wavelength. The thicknesses calculated for the reflectors fabricated by Kung et al. [25] are given for comparison.

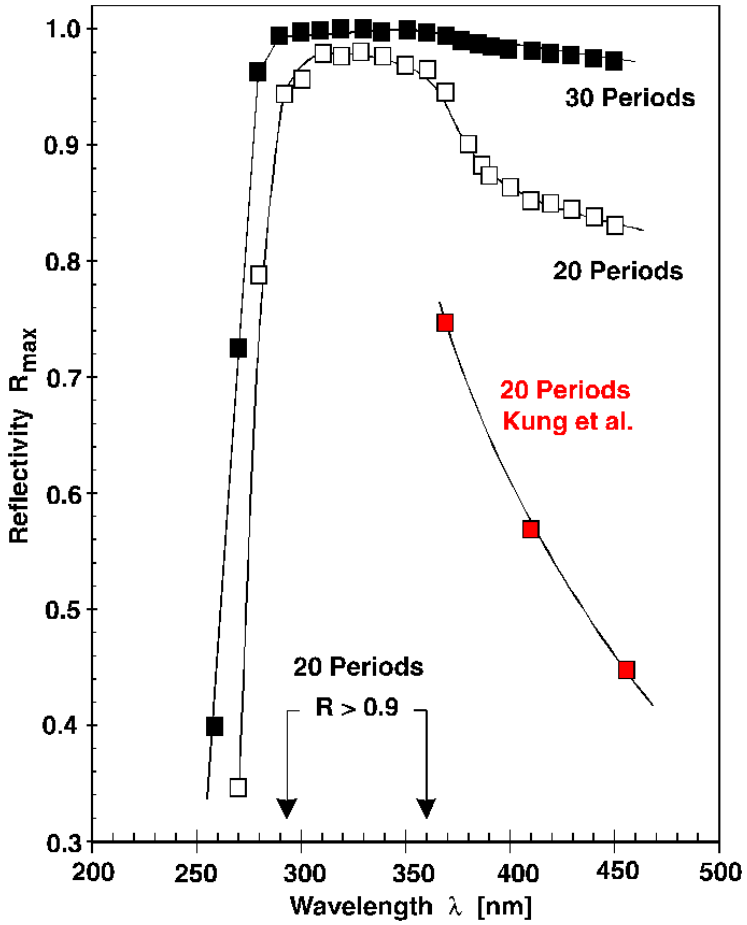

Figure 8. Calculated maximum reflectivity of the AlGaN-based Bragg reflectors with 20 and 30 periods of $Al_{x1}Ga_{1-x1}N/Al_{x2}Ga_{1-x2}N$. The reflectivities calculated for the reflectors fabricated by Kung et al. [25] are given for comparison.

https://doi.org/10.1557/S1092578300001484 Published online by Cambridge University Press

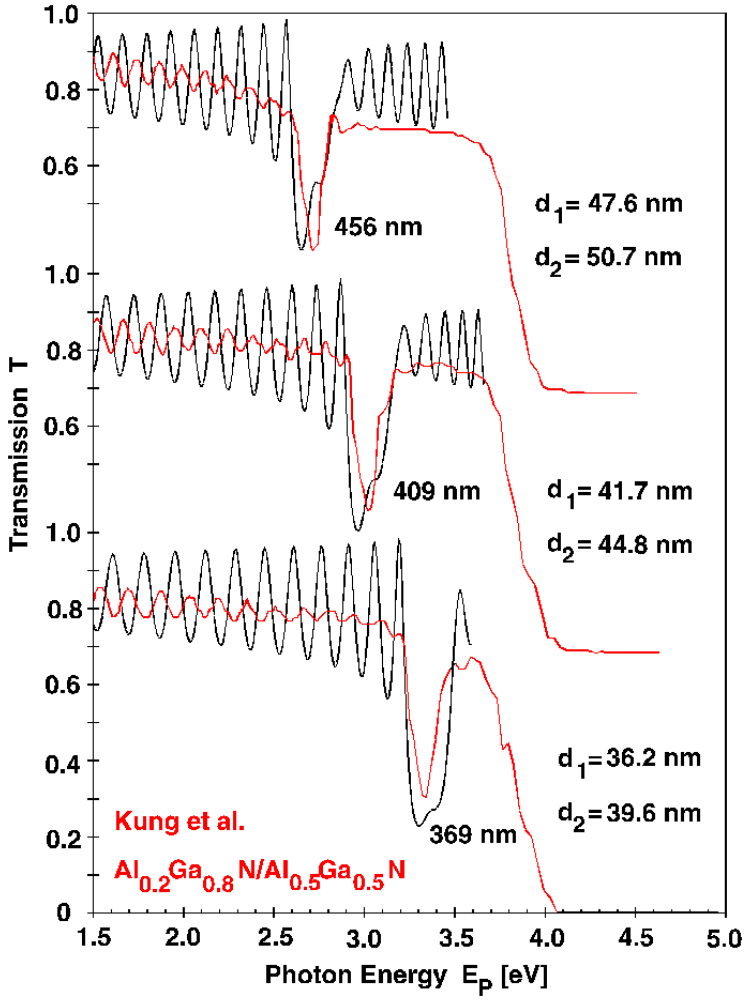

Figure 9. Simulation of the transmission spectra of Bragg reflectors obtained by Kung et al. [25]

https://doi.org/10.1557/S1092578300001484 Published online by Cambridge University Press